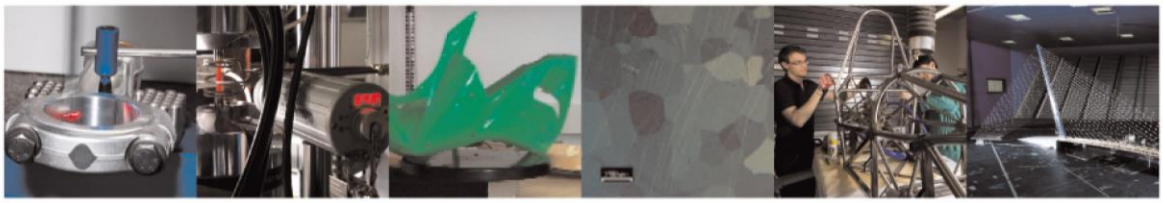

Simulation of edge quality in fused deposition modeling

Armillotta, A.

This is a post-peer-review, pre-copyedit version of an article published in Armillotta, A. (2019), "Simulation of edge quality in fused deposition modeling", Rapid Prototyping Journal, Vol. 25 No. 3, pp. 541-554. The final authenticated version is available online at: http://dx.doi.org/10.1108/RPJ-06-2018-0151

DIPARTIMENTO DI MECCANICA ■ POLITECNICO DI MILANO
via G. La Masa, 1 ■ 20156 Milano ■ EMAIL (PEC): pecmecc@cert.polimi.it
http://www.mecc.polimi.it
Rev. 0

Simulation of edge quality in Fused Deposition Modeling

Abstract
Purpose – A method is proposed for simulating the profile of part edges as a result of the FDM process. Deviations from nominal edge shape are predicted as a function of the layer thickness and three characteristic angles depending on part geometry and build orientation.
Design/methodology/approach – Typical patterns of edge profiles were observed on sample FDM parts, and interpreted as the effects of possible toolpath generation strategies. An algorithm was developed to generate edge profiles consistent with the patterns expected for any combination of input variables.
Findings – Experimental tests confirmed that the simulation procedure can correctly predict basic geometric properties of edge profiles such as frequency, amplitude and shape of periodic asperities.
Research limitations/implications – The algorithm takes into account only a subset of the error causes recognized in previous studies. Additional causes could be integrated in the simulation to improve the estimation of geometric errors.
Practical implications – Edge simulation may help avoid process choices that result in aesthetic and functional defects on FDM parts.
Originality/value – Compared to statistical estimation of geometric errors, graphical simulation allows a more detailed characterization of edge quality and a better diagnosis of error causes.

Keywords
Additive manufacturing; Fused deposition modeling; accuracy; detail resolution.

1 Introduction

Edges are visually relevant features in manufactured parts. When defects and geometric errors spoil the appearance of an edge, the perceived quality of the product can be seriously impaired. This may be more of an issue with additive manufacturing (AM) due to several reasons: the layerwise fabrication creates discontinuities on part features, the lack of dedicated tooling does not allow a full control of material flow during the process, and no finishing treatments are usually planned to correct the manufacturing errors.
The paper deals with the estimation of the geometric deviations on an edge as a function of part geometry and process choices. The focus is on the Fused Deposition Modeling (FDM) process, widely used for the prototyping and the direct manufacture of parts in thermoplastic materials. The detail resolution of FDM has been steadily improving over time, but is still lower than other AM techniques in the search of an optimal balance with build time. Therefore, the accuracy and surface quality of FDM parts have been thoroughly studied in order to understand the error causes and reduce their effects through process planning (Turner et al., 2014; Turner and Gold, 2015). Attention has mainly been given to generic surface features, which share some of the quality issues of edges.
The accuracy of the process was initially evaluated through dimensional and geometric measurements on benchmark parts built with varying process settings. The parts were either simple primitive shapes (Ziemian and Crawn, 2001; Pérez, 2002; Wang et al., 2007; Noriega et al., 2013), collections of features of different shapes and dimensions (Bakar et al., 2010; Johnson et al., 2014), or functional parts from real products (Singh, 2014). Analytic models and numerical simulations have then been developed to describe the main causes of geometric errors, including layer discretization (Chen and Feng, 2011), inaccuracies on machine drives (Agrawal and Dhande, 2007; Tong et al., 2008), vibration of the deposition head (Duan et al., 2017), warpage due to differential shrinkage (Wang et al., 2007; Zhang and Chou, 2008; Sood et al., 2009; Kantaros

and Karalekas, 2013; Peng et al., 2014; Xinhua et al., 2015; Panda et al., 2017; Armillotta et al., 2018; Fitzharris et al., 2018; Li et al., 2018), and the stackup of flatness errors from layer to layer (Boschetto and Bottini, 2014; Volpato et al., 2014).

The surface texture induced by layer discretization has also been investigated. Experiments based on roughness measurements have been carried out for different purposes, including the statistical evaluation of the effects of process variables (Anitha et al., 2001; Campbell et al., 2002; Mahapatra and Sood, 2012; Boschetto et al., 2012; Barari et al., 2017; Taufik and Jain, 2017), the development of geometric models for error prediction (Masood et al., 2000; Ahn et al., 2005; Ahn et al., 2009; Panda et al., 2016; Di Angelo et al., 2017; Vahabli and Rahmati, 2017; Lalehpour and Barari, 2018), the comparison of the surface finish achievable with different machines (Li et al., 2017), and the optimization of surface finish by process planning (Thrimurthulu et al., 2004; Ghorpade et al., 2007; Ingole et al., 2011; Boschetto et al., 2013; Taufik and Jain, 2016).

The importance of edge quality has been recently recognized in the manufacture of anatomical models from computer tomography scans, which typically include many edges to be faithfully reconstructed for diagnostic purposes. In (Ide et al., 2017), edge defects are evaluated on sample parts built in different orientations on different FDM machines.

(Armillotta and Cavallaro, 2017) highlight some specific aspects of edges compared to surface features. The most important is that errors depend on a wider set of variables, which include three characteristic angles rather than only one (the inclination angle) applying to surfaces. Consequently, more error causes may be recognized for edges: in (Armillotta et al., 2017), measurements of edge profiles on FDM parts lead to identify some causes that are either common to surfaces (staircasing, damage due to supports), or exclusive to edges (rounding and offsetting of deposition trajectories), or common to surfaces but not previously discussed (deviations on horizontal edges due to discrete-thickness slicing and material swelling).

Moving from the results of previous studies, this paper proposes a method for the graphical simulation of edge profiles in FDM parts. The observation of samples built with different characteristic angles has helped recognize typical patterns of profiles, which are related to a primary subset of the above cited error causes. An algorithm has been developed to generate these patterns for straight-line edges with given layer thickness and characteristic angles. The generated profiles have been compared to experimental measurements in order to quantify the effects of secondary error causes neglected in the simulation procedure.

2 Previous results

The work retains some basic assumptions of previous studies contributed to by the author (Armillotta and Cavallaro, 2017; Armillotta et al., 2017). These include the use of industrial-grade FDM machines, where two thermoplastic resins (build material and support material) are deposited through two vertical extrusion nozzles onto a horizontal build platform, and the whole build volume is enclosed in a heated chamber. The input to the process is a digital model in STL format, which approximates the surface of the part by triangle facets. Once the user has selected a build orientation for the part, the control software drives the FDM machine by calculating the contours of the layers (slicing) and the trajectories of the deposition head relative to the build platform (toolpath generation).

The quality of an edge is assumed to depend on the following variables (Fig. 1):

- the layer thickness s;
- the inclination angle α between the tangent unit vector **t** of the edge and the horizontal plane;
- the included angle β between the two adjacent facets in a plane perpendicular to the edge;
- the incidence angle γ between the normal unit vector **n** of the edge and the horizontal plane.

Between the two possible directions, **t** points upwards (or horizontally), while **n** points away from the material. Additional influence factors may include the two deposited materials, the way of removing the

supports (break-away or soluble), process temperatures and speeds, and infill parameters. They are usually thought to play a secondary role in the accuracy of FDM parts, and will not be considered here.

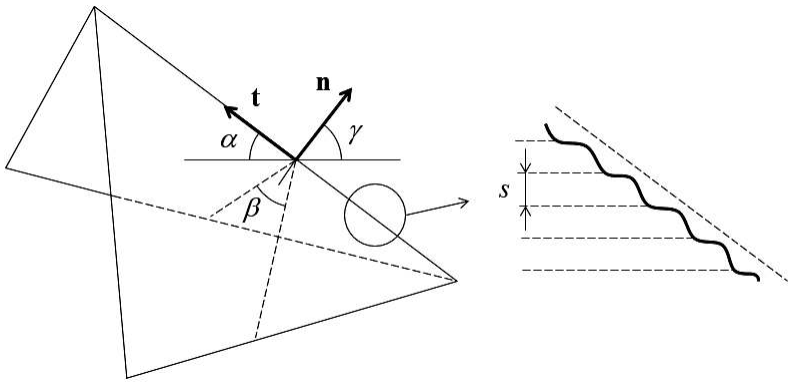

Fig. 1: Geometric variables associated with an edge

The quality of an edge (assumed rectilinear and convex) can be evaluated by measuring its profile on the plane of vectors **t** and **n** (Fig. 2). The distances z of the points of the profile from the nominal profile vary periodically due to layer transitions. Assuming that the regression line of the measured profile is parallel to the nominal profile, two geometric errors on the edge are considered:

- the position error E_P, equal to the average distance of the points from the nominal profile;
- the form error E_F, equal to the root-mean-square (RMS) deviation of the same distances.

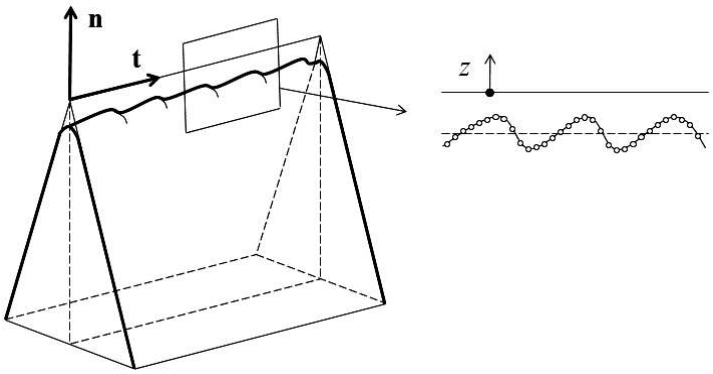

Fig. 2: Geometric errors on an edge

Experimental tests with fixed layer thickness s have shown that especially large values of errors E_P and E_F occur for particular combinations of the characteristic angles α, β and γ. These adverse conditions have been associated to the following error causes:

- *staircase*: the periodic variation of the profile due to the stacking of layers;
- *radius*: the displacement of the edge along **–n** due to a rounded bend in the deposition trajectory;
- *offset*: the displacement along **n** of a sloped edge because the toolpath gets too close to the nominal surface;
- *support*: the perturbations on the profile due to the removal of the supports after the build process, or to any other interaction between support and build material;
- *slicing*: the displacement along **–n** of a horizontal edge because of the limited set of vertical heights available due to the stacking of layers;
- *swelling*: the displacement along **n** of a horizontal edge because the material expands to recover the compressive stress accumulated during the extrusion.

The first three causes can be more easily predicted from the edge variables, and their effects will be modeled in the proposed simulation procedure.

3 Analysis of edge profiles

The objective of this work is the simulation of edge profile for any possible combination of input variables s, α, β and γ. Compared to previous studies, this requires a deeper understanding of the effects of the primary error causes. Some results in this direction derive from the observation of typical profile patterns and deposition toolpaths on FDM parts.

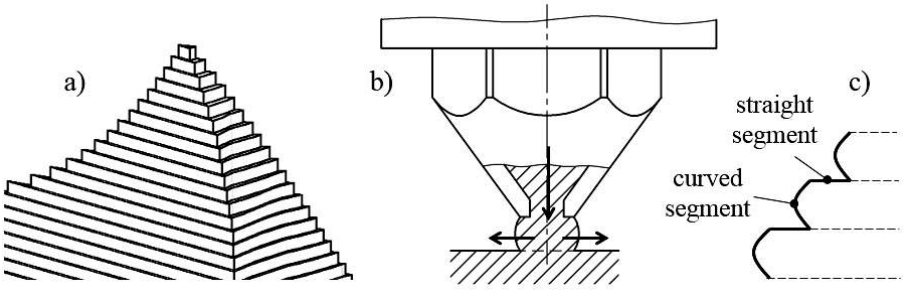

Fig. 3: Staircase effect: a) simplified visualization, b) curved free boundary, c) features of edge profile

The most notable artifacts on the surface of FDM parts are the step-like asperities due to the layer structure. For edges, these defects can be even more visible on the silhouette of the part. In a simplified visualization of the staircase effect (Fig. 3a), the layers are assumed to have straight boundaries, which would appear as straight-line segments in a section on the profile plane. At a closer look, however, the assumption of straight layer boundaries appears too simplistic, as the cross section of the bead of deposited material has a curved free boundary (Fig. 3b). This is because the extruded material is pressed between the tip of the nozzle and the underlying layer, and flows sideways while adhering to the horizontal constraining surfaces.

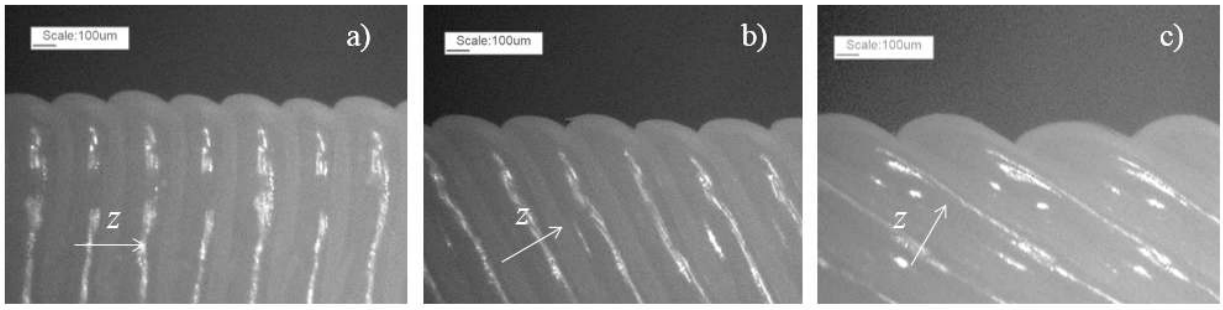

Fig. 4: Curved staircasing: a) $\alpha = 90°$, b) $\alpha = 60°$, c) $\alpha = 30°$

The curved free boundaries create asperities even on vertical edges that would appear as perfect in the simplified visualization. For example, the profile of the vertical edge in Fig. 4a ($\alpha = 90°$, $\beta = 30°$, $\gamma = 0°$) is a sequence of curved segments whose height is about 50 µm, around 20% of layer thickness (s = 0.254 mm). On sloped edges ($0° < \alpha < 90°$), the profile should include curved segments alternating with straight segments created by layer planes (Fig. 3c); actually, the curved boundary of a layer tends to follow the slope of the edge, probably because the extruded bead is dragged by the underlying plastic, i.e. sticks to it more than to the metal nozzle. On the edge in Fig. 4b ($\alpha = 60°$, $\beta = 30°$, $\gamma = 30°$), the curved asperities seem to be rotated with respect to the layer plane, and there is no straight segment; the height of the asperities is thus smaller than it could be expected without the rotation. The drag effect has a limit when α decreases: in Fig. 4c ($\alpha = 30°$, $\beta = 30$, $\gamma = 60°$), the curved portion of the profile does not completely follow the slope of the

edge, and a straight-line segments appears. Based on observations, it can be roughly assumed that the drag shortens the straight-line segments by a maximum length in constant ratio with layer thickness. Finally, horizontal edges do not obviously have any staircasing as they are deposited in a single layer, so they have only very small form errors arising from random variation of bead thickness.

The deposition toolpaths at edges give further insights for predicting the geometric errors. As a first example, Fig. 5a shows an edge on the plane perpendicular to the tangent vector **t** ($\alpha = 90°$, $\beta = 60°$, $\gamma = 0°$) overlaid to the slicing contour (two straight lines at an angle of 60°). The width of the deposited bead is set at twice the layer thickness (i.e. 0.508 mm for s = 0.254 mm). Although the actual toolpath generation algorithm is not publicly disclosed, it is likely that the layer boundaries are kept as close as possible to the nominal surface; therefore, it can thus be assumed that the toolpath is offset inward by a distance equal to half the width, i.e. the layer thickness. At an edge, the toolpath bends on the layer plane by an angle $\beta' \leq \beta$ (as β is defined in a plane normal to the edge). As a first approximation, the bead can be assumed to have constant width; possible changes due to accelerations of the deposition head may occur but could not be recognized in microscopic observations. As a consequence, the outer contour of the bead takes a circular shape with radius equal to the offset distance s (Fig. 5b).

Fig. 5c shows an edge with small included angle ($\alpha = 90°$, $\beta = 30°$, $\gamma = 0°$). The contour of the bead seems to cross the slicing contour toward the outside. This may be an effect of a toolpath generation strategy aimed to control the position error, i.e. the distance between the bead and the nominal edge. The error increases when s increases and the β' decreases. When β' is small, the toolpath is apparently corrected to avoid that the position error becomes very large (Fig. 5d): the observation of different cases suggests that the incoming and outgoing lines of the toolpath diverge slightly from the slice contours to ensure that the bend angle never falls below a certain limit β_0 (seemingly close to 45°). One possible assumption is that the extensions of the outer contours of the bead intercept a segment of fixed length (about s / 3) on the nominal contour of the layer. As a consequence, the position error increases as β' decreases but more gradually than expected from the general scheme.

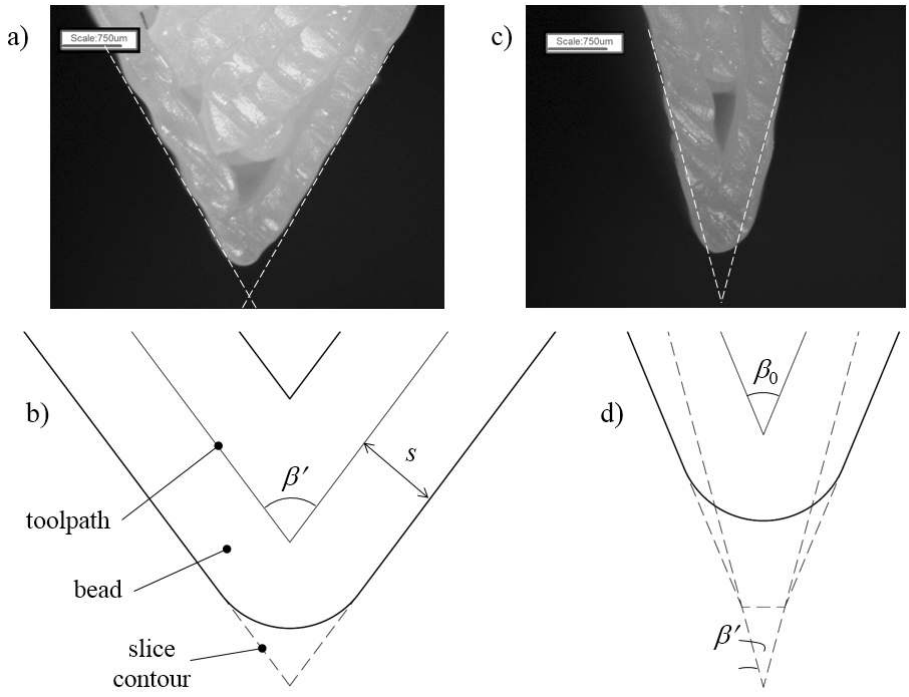

Fig. 5: Toolpaths at edges: a) edge with $\beta = 60°$; b) offset toolpath; c) edge with $\beta = 30°$; d) possible correction of the toolpath for small angles

4 Generation of edge profile

The above discussed geometric effects are considered in the simulation procedure, which consists in the three phases described below.

4.1 Setup of the profile plane

The unit vectors associated with the edge are constructed in the origin of the *xyz* coordinate system of the build chamber (Fig. 6a). The tangent **t** lays in the *xz* plane with an angle α to the *x* axis. The normal **n** is obtained in two steps: first, **t** is rotated about the *y* axis by −90° obtaining a unit vector $\mathbf{n_0}$ in the *xz* plane; then, if $0° < \alpha < 90°$, $\mathbf{n_0}$ is rotated about **t** by an angle ζ (azimuth), which is calculated by the following condition:

$$\sin\gamma = \cos\alpha \cdot \cos\zeta$$

The plane of **t** and **n** is the profile plane, whose intersection with the *xy* plane gives the layer direction

$$\mathbf{d} = \frac{(\mathbf{n} \wedge \mathbf{t}) \wedge \mathbf{k}}{|(\mathbf{n} \wedge \mathbf{t}) \wedge \mathbf{k}|}$$

where **k** is the unit vector of the *z* axis. If $\alpha > 0°$, lines corresponding to consecutive layers can be constructed by repeatedly displacing **d** by the following translation vector parallel to **t**:

$$\mathbf{p} = p\mathbf{t} = \frac{s}{\sin\alpha}\mathbf{t}$$

whose length *p* is the spacing of the periodic asperities of the profile (Fig. 6b).

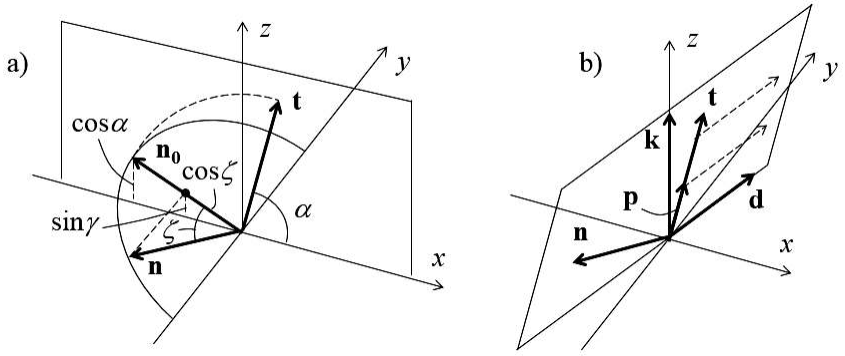

Fig. 6: Construction of characteristic directions: a) azimuth angle; b) direction of layers

Said $\mathbf{f_1}$ and $\mathbf{f_2}$ the unit vectors obtained by rotating −**n** about **t** by angles $\beta/2$ and $-\beta/2$, similar expressions give two unit vectors $\mathbf{g_1}$ and $\mathbf{g_2}$ parallel to the edge faces on the layer contour:

$$\mathbf{g_1} = \frac{(\mathbf{f_1} \wedge \mathbf{t}) \wedge \mathbf{k}}{|(\mathbf{f_1} \wedge \mathbf{t}) \wedge \mathbf{k}|}, \quad \mathbf{g_2} = \frac{(\mathbf{f_2} \wedge \mathbf{t}) \wedge \mathbf{k}}{|(\mathbf{f_2} \wedge \mathbf{t}) \wedge \mathbf{k}|}$$

The nominal bend angle of the toolpath is thus given by

$$\cos\beta' = \mathbf{g_1} \cdot \mathbf{g_2}$$

Fig. 7a shows all the above vectors in three-dimensional view. For a more convenient display of edge profile, they are transformed so as to bring **t** parallel to *x* and **n** parallel to *z*. This requires two successive rotations, the first about **t** by angle $-\zeta$, the second about the *y* axis by angle α. Fig. 7b shows the transformed vectors **t′**, **n′**, **d′** and **p′** in two-dimensional view. The angle φ between the layers and the edge is such that

$$\cos\varphi = \mathbf{d}' \cdot \mathbf{t}'$$

and the thickness of the layers on the profile plane is given by

$$s_n = p \sin\varphi$$

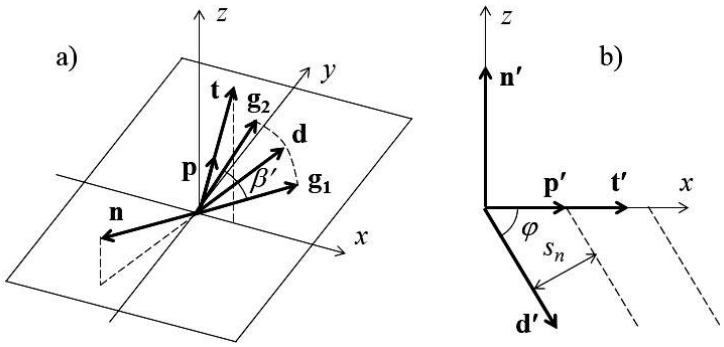

Fig. 7: Characteristic directions: a) three-dimensional view; b) transformation of the profile plane

4.2 Position and height of the profile

To simulate the position error, $\mathbf{t}'$ must be translated along $\mathbf{d}'$ by a distance d_r related to the radius effect discussed in the previous section. If $\alpha = 0°$, the edge is created on a single layer with a straight toolpath, hence $d_r = 0$. In the other cases, the distance is calculated by graphical constructions of the outer profile of the bead, distinguishing the case of small angles requiring the correction of the bend angle (Fig. 8):

$$d_r = \begin{cases} s\left(\dfrac{1}{\sin\beta'/2} - 1\right), & \beta' \geq \beta_0 \\ s\left(\dfrac{1}{\sin\beta_0/2} - 1\right) + \dfrac{u}{2}\left(\dfrac{1}{\tan\beta'/2} - \dfrac{1}{\tan\beta_0/2}\right), & \beta' < \beta_0 \end{cases}$$

where β_0 is the minimum bend angle, and u is the intercept of the actual contour lines (with angle β_0) and the contour lines obtained by slicing (with angle β') when $\beta' < \beta_0$. While not excluding more complex strategies for toolpath generation, fixed values will be assumed for these two parameters ($\beta_0 = 45°$, $u = s / 3$).

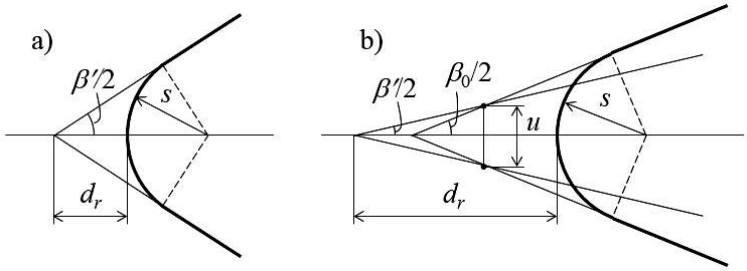

Fig. 8: Displacement of the profile: a) $\beta' \geq \beta_0$, b) $\beta' < \beta_0$

Next, the height h of the periodic asperities along $\mathbf{d}'$ is estimated. The case $\alpha = 0°$ is trivial, since the simulated profile will be a straight line with $h = 0$. In other cases, the shape of the asperities depends on the curvature of the bead in the vertical planes (curved free boundary) and in the horizontal plane (radius effect). The height will be calculated simply as a superposition of partial heights related to the two distinct effects:

$$h = h_1 + h_2$$

To estimate h_1 and h_2, special cases are considered where one of the two effects vanishes. When $\zeta = 0°$ (i.e. $\gamma = 90° - \alpha$) or $\zeta = 180°$ (i.e. $\gamma = \alpha - 90°$), the profile plane is vertical and the shape of the profile depends only on the curvature of the free boundary (Fig. 9). The partial height h_1 due to this effect equals the sag of the arc in the cross section of the bead, which is assumed as a fixed fraction $k = 0.2$ of layer thickness:

$$h_1 = ks$$

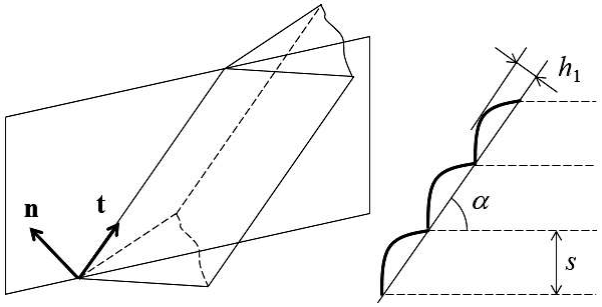

Fig. 9: Profile height due to the curved free boundary

When $\zeta = 90°$, the edge is side-facing and shape of the profile depends only on the radius effect (Fig. 10). On the layer plane, the outer contour of the bead can be approximated with a circular arc with radius s tangent to two straight segments forming an angle β'. This determines the shape of the profile for a width

$$w = \frac{s}{\tan\alpha}$$

which must be compared with the chord of the arc

$$w_a = 2s\cos\beta'/2$$

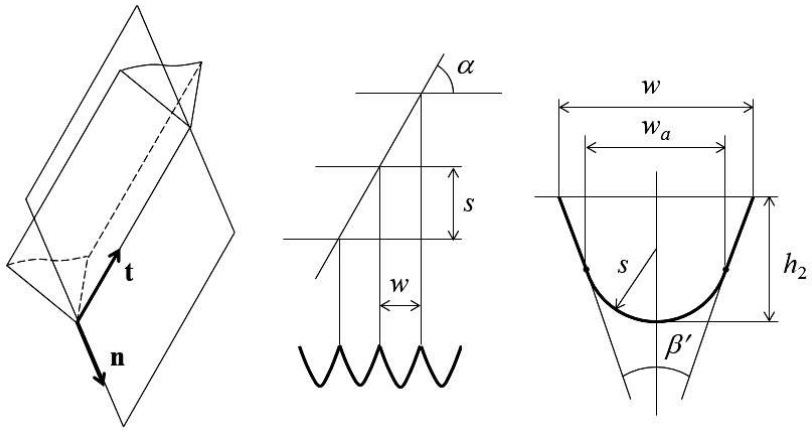

Fig. 10: Profile height due to the radius effect on side-facing edges

If $w < w_a$, the profile includes an arc with radius s and chord w, whose sag is equal to

$$(h_2)_0 = s - \sqrt{s^2 - \frac{w^2}{4}} = s\left(1 - \sqrt{1 - \frac{1}{4\tan^2\alpha}}\right)$$

If $w = w_a$, the profile extends to the whole arc between the two tangency points, and its height is

$$(h_2)_0 = s - \sqrt{s^2 - \frac{w_a^2}{4}} = s(1 - \sin\beta'/2)$$

If $w > w_a$, the profile includes also two straight-line segments, and its height is

$$(h_2)_0 = s\left(1 - \sin\beta'/2 + \frac{1 - 2\tan\alpha\cos\beta'/2}{2\tan\alpha\tan\beta'/2}\right)$$

This expression has to be corrected as the corner between the straight lines of two adjacent asperities is actually rounded off, probably due to the free flow of molten material in unsupported areas (bridging). This further effect is less easy to describe without resorting to physical properties of the material, and will be tentatively accounted for by applying a factor $f_r = 0.3$ to the height of the straight lines:

$$(h_2)_0 = s\left(1 - \sin\beta'/2 + f_r\frac{1 - 2\tan\alpha\cos\beta'/2}{2\tan\alpha\tan\beta'/2}\right)$$

For different values of ζ, the height of the profiles will be approximated by the following expression

$$h_2 = (h_2)_0 \sin\zeta = \begin{cases} s\sin\zeta\left(1 - \sqrt{1 - \dfrac{1}{4\tan^2\alpha}}\right), & \tan\alpha \geq \dfrac{1}{2\cos\beta'/2} \\ s\sin\zeta\left(1 - \sin\beta'/2 + f_r\dfrac{1 - 2\tan\alpha\cos\beta'/2}{2\tan\alpha\tan\beta'/2}\right), & \tan\alpha < \dfrac{1}{2\cos\beta'/2} \end{cases}$$

which satisfies those found for the previous cases ($\zeta = 0°, 90°, 180°$).

4.3 Construction of the profile

The staircase effect with curved layer boundary now has to be simulated. As a first approximation (Fig. 11a), two valley points with spacing s_n are constructed along x, and a peak point is constructed in between at a distance h from x. The three points are interpolated with a quadratic curve, which is then rotated by an angle ($90° - \varphi$) and translated along $\mathbf{d'}$ by a distance ($d_r + h$), obtaining a single period of the profile. This is finally replicated in a horizontal array with spacing p, adding straight connecting segments to restore the continuity of the profile. Each segment is parallel to $\mathbf{d'}$ and has a length

$$l = \frac{s_n}{\tan\varphi}$$

To introduce the drag effect (Fig. 11b), the quadratic curve is adjusted by reducing the connecting lengths by a maximum value l_0 assumed equal to s. For this purpose, the two endpoints of the curve are moved vertically before the rotation by a distance

$$\delta l = \begin{cases} l/2, & l \leq l_0 \\ l_0/2, & l > l_0 \end{cases}$$

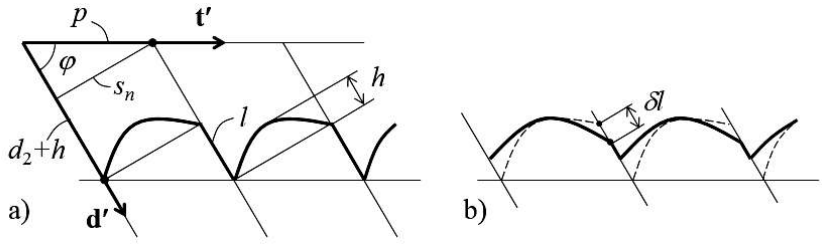

Fig. 11: Construction of profiles: a) simple staircasing; b) staircasing with drag

Fig. 12 shows an example of edge profile generated by the described procedure. The display includes the nominal profile at $z = 0$, and three periods of the simulated profile with the traces of layer planes. The sample

mean and standard deviation of the z coordinates of profile points are calculated as estimates of position error E_P and form error E_F.

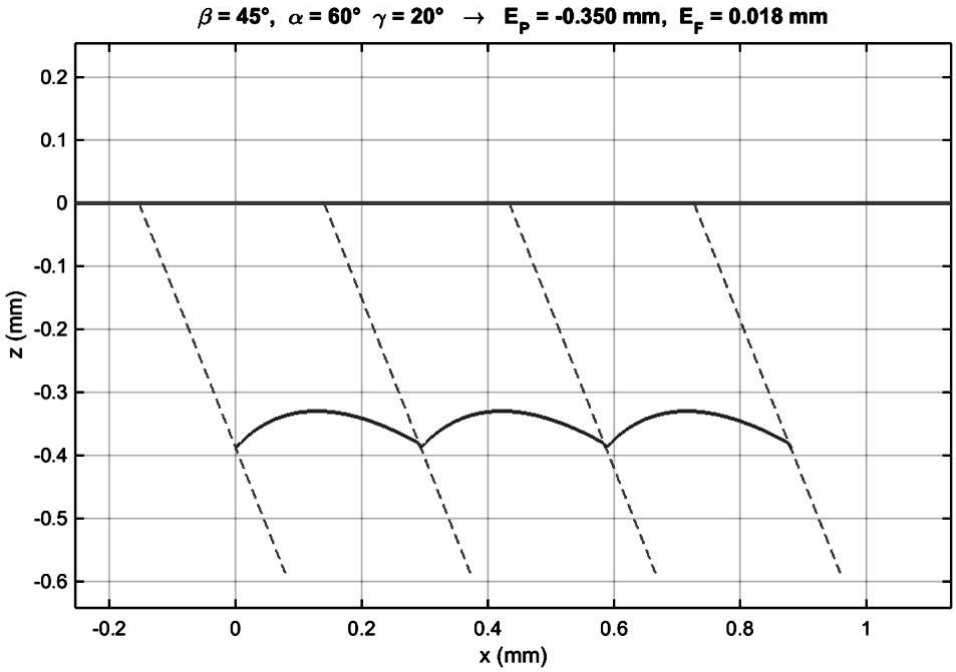

Fig. 12: Visualization of a simulated profile

5 Results

The simulation procedure was validated using the experimental results of (Armillotta et al., 2017), where sample parts were built in acrylonitrile butadiene styrene (ABSplus-P430) on a Stratasys Fortus 250mc machine with s = 0.254 mm. The experiment was designed as a full factorial plan in three variables with levels β = 30°/60°/90°/120°, α = 0°/30°/60°/90°, and γ = 0°/(90°−α)/−(90°−α), and with 3 replications for each combination of levels. On each sample part, the profile of the edge was measured by a Mitutoyo QV-ELF202 optical measuring instrument for 2D profiles with a resolution of 40 µm and a stated accuracy of 2 µm. The points of the profile were then analyzed by a Matlab script in order to evaluate errors E_P and E_F. In the following, the collected data are compared to the profile and to the errors predicted by simulation for the same values of s, α, β and γ.

Position errors E_P were in the range between −0.6 and 0.5 mm. Their differences from simulated values $(E_P)_{sim}$ have an average of 0.03 mm and an RMS deviation of 0.17 mm; these statistics exclude three outliers which were probably due to measurement errors. Fig. 13 compares E_P and $(E_P)_{sim}$, confirming that the variation of the experimental values is generally centered on the simulated values and limited within a range of ±0.2 mm for $\alpha \neq 0°$. Horizontal edges are not affected by the staircase and radius effects, thus the simulation estimates a zero position error; on the sample parts, however, E_P varies between −0.3 and 0.5 mm. The difference can be attributed to error causes neglected by the simulation. One of these is the slicing effect, which bounds the actual position of a horizontal edge to a finite set of heights multiple of the layer thickness; depending on the distance of the edge to the build platform, which is determined by part size and angle γ, the actual edge could depart from the nominal position by a maximum amount of s (0.254 mm in this case). Another one is the swelling of the material, which displaces the edge to the outside of the part, generally leading to positive position errors; this might explain the positive average of the differences for α = 0°.

In Fig. 14, the differences are plotted as a function of α and

$$\delta = 90° - \gamma - \beta/2$$

which is the angle between the lower face of the edge and the vertical plane. If $\delta > 0°$, as it is the case for small values of γ and β, the edge is a overhung feature not supported by the underlying material during build. If δ exceeds a certain value (probably ≈ 50° for the used machine), support material has to be deposited to prevent the collapse of the build material by gravity. The plot suggests that the presence of supports, whose effects were not accounted for in the simulation, has a minor effect on the position error. This can be possibly recognized in the slightly larger differences for equal α when supports are needed.

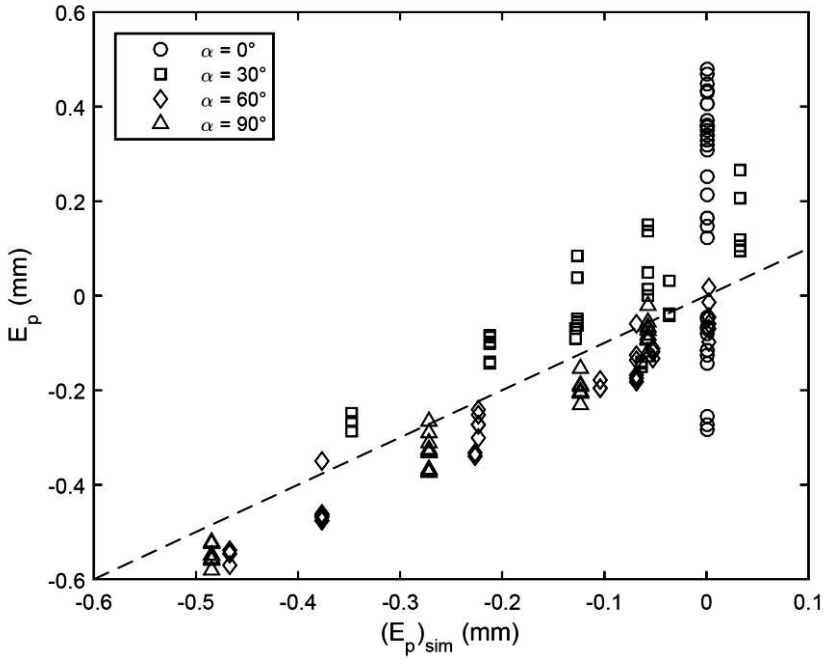

Fig. 13: Comparison of experimental and simulated position errors

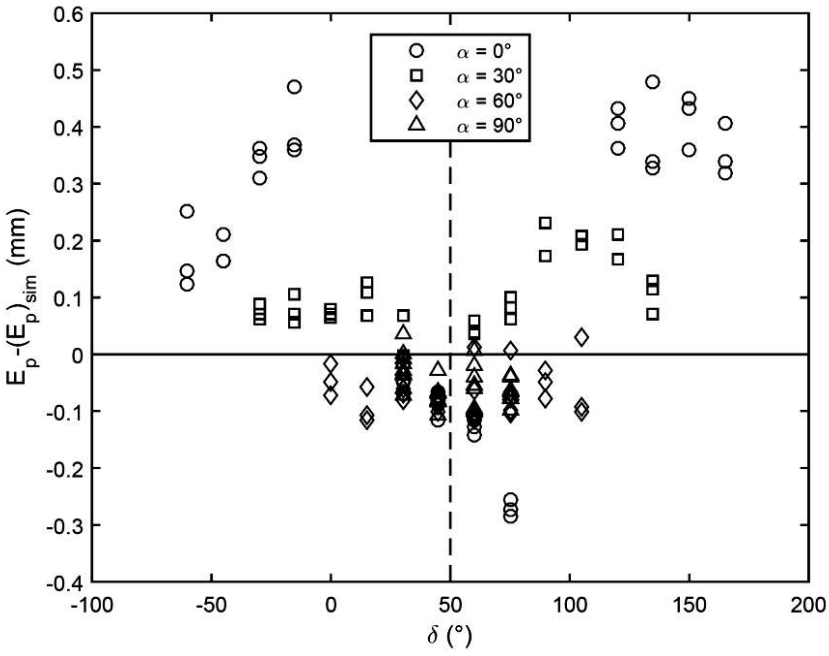

Fig. 14: Analysis of differences between experimental and simulated position errors

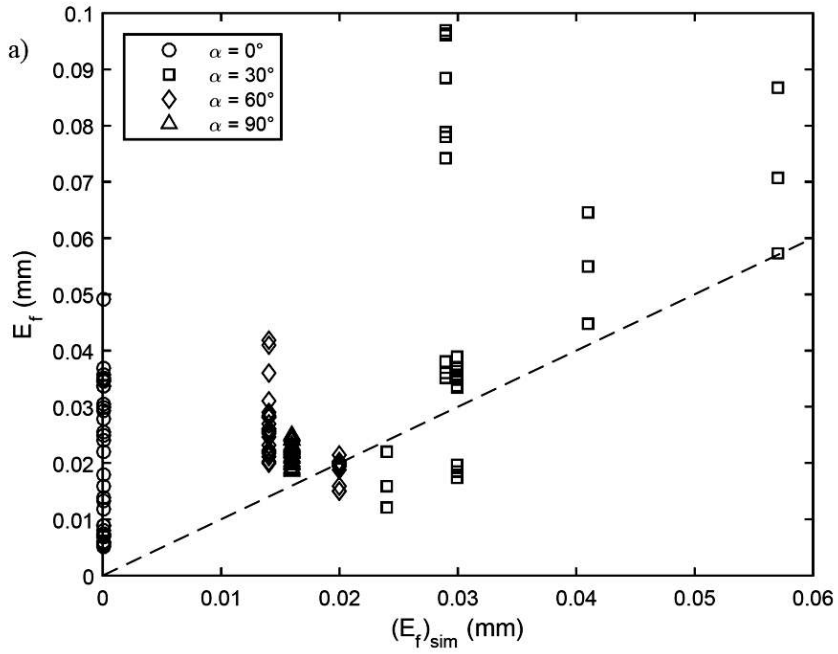

Fig. 15: Comparison of experimental and simulated form errors

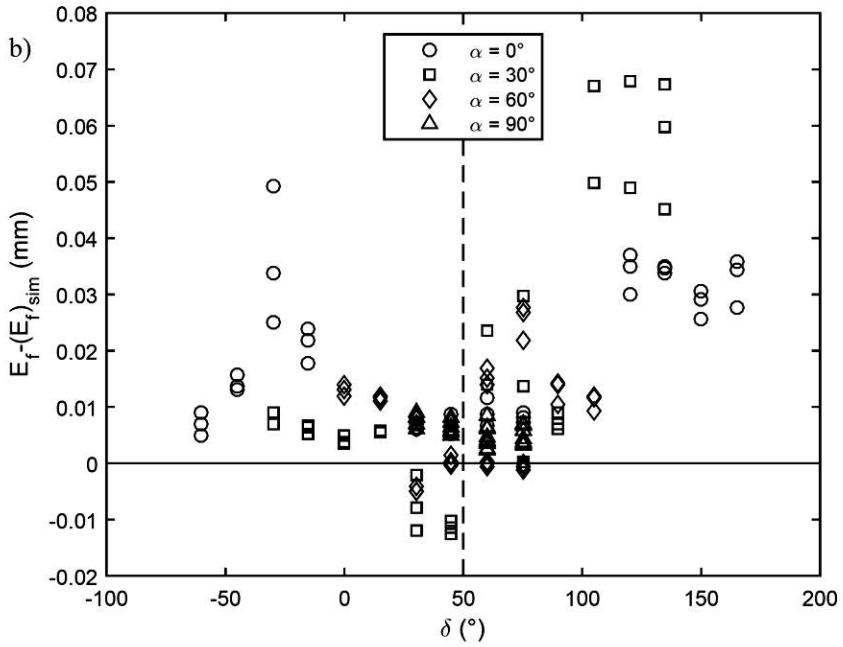

Fig. 16: Analysis of differences between experimental and simulated form errors

Form errors E_F were in the range between 0 and 0.1 mm. Their differences from simulated values $(E_F)_{sim}$ have an average of 0.013 mm and an RMS deviation of 0.016 mm. The comparison in Fig. 15 shows than, except for a limited number of conditions, the estimation of the form error has a uniform negative bias. This might be partially corrected through an adjustment of the simulation model after further experimental investigations on the amount of form errors due to the curved free boundary of layers. Again, however, the difference could depend on non-geometric error causes; as shown in Fig. 16, the largest differences are found for high values of δ, and thus seem to be explained by the effect of support removal. At a lesser degree, the simulation underestimates the form error for a particular combination of angles ($\beta = 60°$, $\alpha = 0°$, $\gamma = 90°$) where supports are not needed. In addition to the basic issue for horizontal edges (which are simulated as

straight lines), the parts built in these conditions show small local defects of the edge, apparently due to the leak of a small amount of extruded resin during a pause of the deposition.

The correctness of the simulation regarding the shape and size of edge profiles is demonstrated in Fig. 17, where actual and simulated profiles are compared for some of the typical cases discussed so far. These include horizontal edges (Fig. 17a), stair-stepped edges with partial drag (Fig. 17b) and with complete drag (Fig. 17c), and side-facing edges (Fig. 17d). For each plot, the two profiles are shown along a 3-mm length after an appropriate registration along the direction of the edge. In all cases, the simulation correctly predicts the spatial frequency and the amplitude of the profile, while the height differences are related to the inaccurate estimation of the position error as previously discussed. The shape of the asperities is reproduced faithfully except in the case in Fig. 17d, where the simulation fails to predict the secondary undulation of the profile over two layers. Using the same scale for the vertical dimensions allows to appreciate the different severity of the form errors and the possible impact on visual appearance.

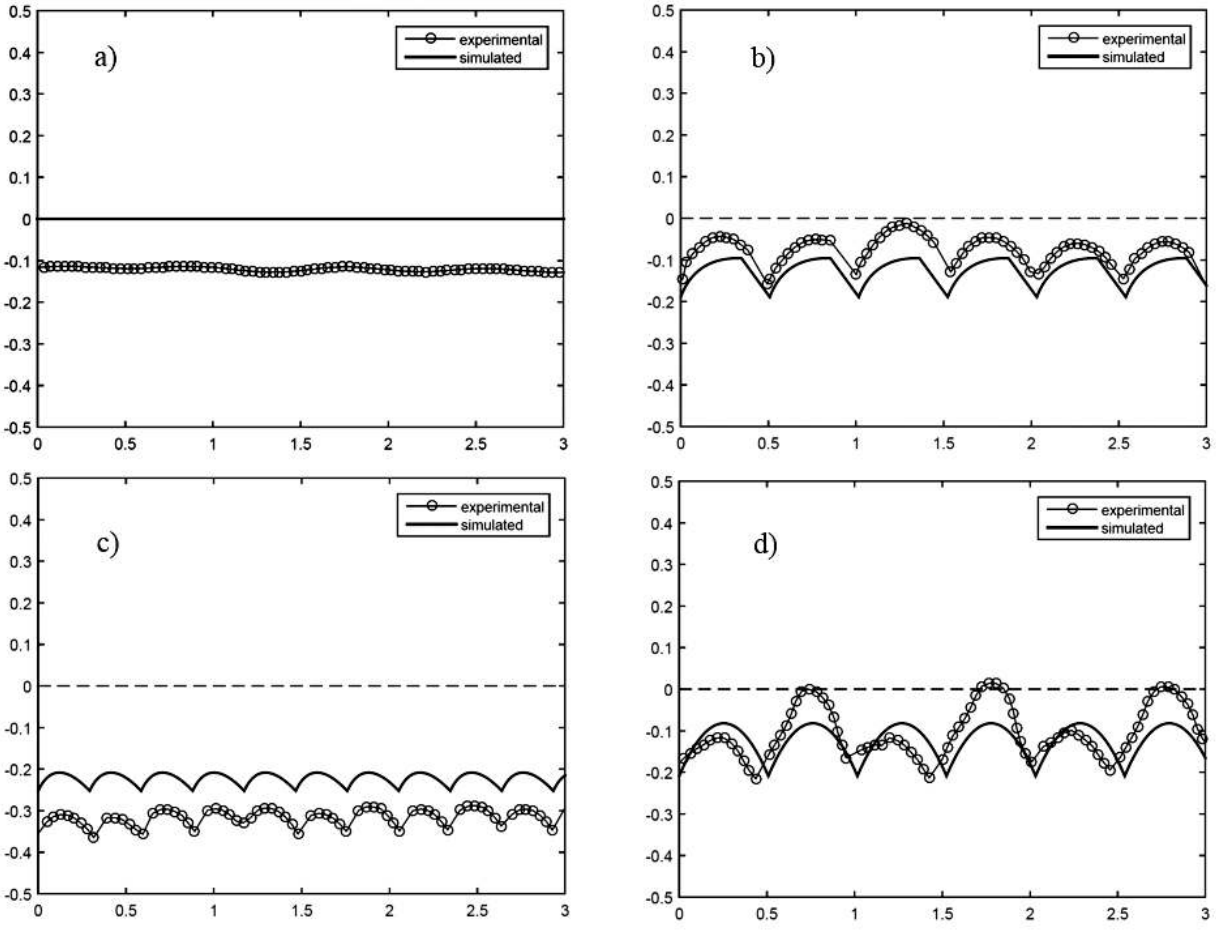

Fig. 17: Comparison of measured and simulated profiles with s = 0.254 mm and β = 60°: a) α = 0°, γ = 0°; b) α = 30°, γ = 60°; c) α = 60°, γ = 30°; d) α = 30°, γ = 0° (dimensions in mm)

The experimental results used for the above comparisons included only a limited subset of the allowable combinations of edge variables. For a further validation, the simulation was run on different process settings. The example in Fig. 18 refers to an edge with a quasi-horizontal direction (α = 15°), where an especially strong staircase effect is expected. The edge has also a different included angle (β = 45°), and its profile plane is not vertical (γ = 30° < 90° − α). The simulated profile is compared with the magnified image of the edge on a sample part built in polycarbonate (PC) on a Stratasys Fortus 400mc machine with a layer thickness s = 0.254 mm, without requiring the deposition of support material (δ = 37.5°). The simulation misses some secondary details in the curved part of the profile, but correctly reproduces its shape, curvature

and proportion with the straight segment between consecutive layer boundaries. Limited to this case, the purely geometric approach to simulation gives qualitatively acceptable results even for a different material to the one (ABS) used in previous tests. This result do neither imply a straightforward extension of those experimental findings, nor lead to assumptions on the influence of material on edge quality.

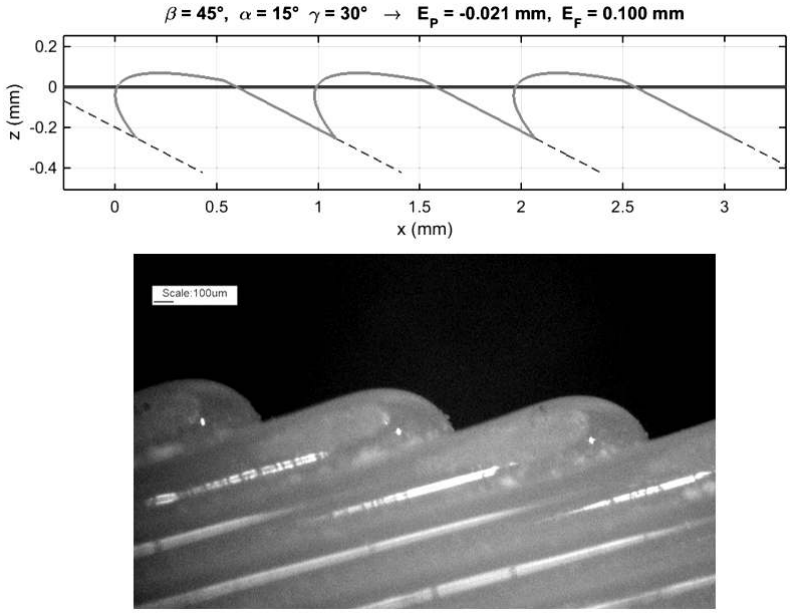

Fig. 18: Verification of simulated profiles with s = 0.254 mm, α = 15°, β = 45°, γ = 30°

6 Conclusions

The paper has proposed a method for simulating the profile of edges on FDM parts. Compared to previous studies, developing the method required a deeper understanding of the causes of geometric errors on edges. Their effects were formalized into a computational procedure that generates a simulated edge profile from a limited set of variables (the layer thickness and the three characteristic angles), which are easily obtained from the STL model of the part rotated in the chosen build orientation. Although the intended value of the work is mostly in the additional insights on how process constraints influence product quality, the simulation can be a helpful tool for evaluating the conformance of the edge to aesthetic or functional requirements.

The simulation procedure was developed considering a subset of the previously identified error causes (staircase, radius, offset), which are purely geometric and thus easier to predict from input data. The validation on FDM sample parts confirmed that these causes are actually prevalent in the prediction of edge shape; among the remaining ones, the slicing and swelling effects have a significant influence on the form error, while the support effect seems to have some effect on the position error. However, it must be acknowledged that even some geometric effects, such as the curvature of the free boundaries of the layers, actually depend on material rheology; a direct modeling of these physical aspects could improve the simulation avoiding the use of adjusting parameters in the construction of edge profiles.

The correctness of the simulation has been mostly verified on experimental data available from a previous study, which cover only a limited fraction of the possible uses of the FDM process. Future developments will include new tests extended to a wider range of materials and process settings, including the use of low-end extrusion-based 3D printers. The collected data will help to improve the modeling of error causes, including those neglected in this work such as bridging. Moreover, the effect of slicing strategies will possibly be accounted for by analyzing available slicing software for FDM. Due to the common error causes, it is expected that further insights for the long-studied quality issues of generic surface features may arise from edge-related results.

Acknowledgements

The author is indebted to Marco Cavallaro, Stefano Bianchi and Stefania Minnella for their support and collaboration in the experimental tests.

References

Agrawal S. and Dhande S.G. (2007), "Analysis of mechanical error in a fused deposition process using a stochastic approach", *International Journal of Production Research*, Vol. 45 No. 17, pp. 3991-4012.

Ahn D.K., Kim H.C. and Lee S.H. (2005), "Determination of fabrication direction to minimize post-machining in FDM by prediction of non-linear roughness characteristics", *Journal of Mechanical Science and Technology*, Vol. 19 No. 1, pp. 144-155.

Ahn D., Kweon J.H., Kwon S., Song J. and Lee S. (2009), "Representation of surface roughness in fused deposition modeling", *Journal of Materials Processing Technology*, Vol. 209, pp. 5593-5600.

Anitha R., Arunachalam S. and Radhakrishnan P. (2001), "Critical parameters influencing the quality of prototypes in fused deposition modelling", *Journal of Materials Processing Technology*, Vol. 118, pp. 385-388.

Armillotta A. and Cavallaro M. (2017), "Edge quality in fused deposition modeling: I. Definition and analysis", *Rapid Prototyping Journal*, Vol. 23 No. 6, pp. 1079-1087.

Armillotta A., Bianchi S., Cavallaro M. and Minnella S. (2017), "Edge quality in fused deposition modeling: II. Experimental verification", *Rapid Prototyping Journal*, Vol. 23 No. 4, pp. 686-695.

Armillotta A., Belotti M. and Cavallaro M. (2018), "Warpage of FDM parts: experimental tests and analytic model", *Robotics and Computer-Integrated Manufacturing*, Vol. 50, pp. 140-152.

Bakar N.S.A., Alkahari M.R. and Boejang H. (2010), "Analysis on fused deposition modelling performance", *Journal of Zheijang University Science A*, Vol. 11 No. 12, pp. 972-977.

Barari A., Kishawy H.A., Kaji F. and Elbestawi M.A. (2017), "On the surface quality of additive manufactured parts", *International Journal of Advanced Manufacturing Technology*, Vol. 89, pp. 1969-1974.

Boschetto A., Giordano V. and Veniali F. (2012), "Modelling micro geometrical profiles in fused deposition process", *International Journal of Advanced Manufacturing Technology*, Vol. 61, pp. 945-956.

Boschetto A., Giordano V. and Veniali F. (2013), "3D roughness profile model in fused deposition modelling", *Rapid Prototyping Journal*, Vol. 19 No. 4, pp. 240-252.

Boschetto A. and Bottini L. (2014), "Accuracy prediction in fused deposition modeling", International *Journal of Advanced Manufacturing Technology*, Vol. 73, pp. 913-928.

Campbell R.I., Martorelli M., Lee H.S. (2002), "Surface roughness visualisation for rapid prototyping models", *Computer-Aided Design*, Vol. 34, pp. 717-725.

Chen J.S.S. and Feng H.Y. (2011), "Contour generation for layered manufacturing with reduced part distortion", *International Journal of Advanced Manufacturing Technology*, Vol. 53, pp. 1103-1113.

Di Angelo L., Di Stefano P. and Marzola A. (2017), "Surface quality prediction in FDM additive manufacturing", *International Journal of Advanced Manufacturing Technology*, Vol. 93, pp. 3655-3662.

Duan M., Yoon D. and Okwudire C.E. (2017), "A limited-preview filtered B-spline approach to tracking control-with application to vibration-induced error compensation of a 3D printer, *Mechatronics*, http://dx.doi.org/10.1016/j.mechatronics.2017.09.002

Fitzharris E.R., Watanabe N., Rosen D.W. and Shofner M.L. (2018), "Effects of material properties on warpage in fused deposition modeling parts", *International Journal of Advanced Manufacturing Technology*, Vol. 95, pp. 2059-2070.

Ghorpade A., Karunakaran K.P. and Tiwan M.K. (2007), "Selection of optimal part orientation in fused deposition modelling using swarm intelligence", *Proceedings IMechE Part B: Journal of Engineering Manufacture*, Vol. 221, pp. 1209-1220.

Ide Y., Nayar S., Logan H., Gallagher B. and Wolfaardt J. (2017), "The effect of the angle of acuteness of additive manufactured models and the direction of printing on the dimensional fidelity: clinical implications", *Odontology*, Vol. 105, pp. 108-115.

Ingole D.S., Deshmukh T.R., Kuthe A.M. and Ashtankar K.M. (2011), "Build orientation analysis for minimum cost determination in FDM", *Proceedings IMechE Part B: Journal of Engineering Manufacture*, Vol. 225, pp. 1925-1938.

Johnson W.J., Rowell M., Deason B. and Eubanks M. (2014), "Comparative evaluation of an open-source FDM system", *Rapid Prototyping Journal*, Vol. 20 No. 3, pp. 205-214.

Kantaros A. and Karalekas D. (2013), "Fiber Bragg grating based investigation of residual strains in ABS parts fabricated by fused deposition modeling process", *Materials and Design*, Vol. 50, pp. 44-50.

Lalehpour A. and Barari A. (2018), "A more accurate analytical formulation of surface roughness in layer-based additive manufacturing to enhance the product's precision", *International Journal of Advanced Manufacturing Technology*, Vol. 96, pp. 3793-3804.

Li Y., Linke B.S., Voet H., Falk B., Schmitt R. and Lam M. (2017), "Cost, sustainability and surface roughness quality-A comprehensive analysis of products made with personal 3D printers", *CIRP Journal of Manufacturing Science and Technology*, Vol. 16, pp. 1-11.

Li H., Wang T., Li Q., Yu Z. and Wang N. (2018), "A quantitative investigation of distortion of polylactic acid (PLA) part in FDM from the point of interface residual stress", *International Journal of Advanced Manufacturing Technology*, Vol. 94, pp. 381-395.

Mahapatra S.S. and Sood A.K. (2012), "Bayesian regularization-based Levenberg-Marquardt neural model combined with BFOA for improving surface finish of FDM processed parts", *International Journal of Advanced Manufacturing Technology*, Vol. 60, pp. 1223-1235.

Masood S.H., Rattanawong W. and Iovenitti P. (2000), "Part build orientations based on volumetric error in fused deposition modelling", *International Journal of Advanced Manufacturing Technology*, Vol. 16, pp. 162-168.

Noriega A., Blanco D., Alvarez B.J. and Garcia A. (2013), "Dimensional accuracy improvement of FDM square cross-section parts using artificial neural networks and an optimization algorithm", *International Journal of Advanced Manufacturing Technology*, Vol. 69, pp. 2301-2313.

Panda B.N., Bahubalendruni R., Biswal B.B. and Leite M. (2016), "A CAD-based approach for measuring volumetric error in layered manufacturing", *Proceedings ImechE Part C: Journal of Mechanical Engineering Science*, Vol. 231 No. 13, pp. 2398-2406.

Panda B.N., Shankhwar K., Garg A. and Jian Z. (2017), "Performance evaluation of warping characteristic of fused deposition modelling process", *International Journal of Advanced Manufacturing Technology*, Vol. 88, pp. 1799-1811.

Peng A., Xiao X. and Yue R. (2014), "Process parameter optimization for fused deposition modeling using response surface methodology combined with fuzzy inference system", *International Journal of Advanced Manufacturing Technology*, Vol. 73, pp. 87-100.

Pérez C.J.L. (2002), "Analysis of the surface roughness and dimensional accuracy capability of fused deposition modelling processes", *International Journal of Production Research*, Vol. 40 No. 12, pp. 2865-2881.

Singh R. (2014), "Process capability analysis of fused deposition modelling for plastic components", *Rapid Prototyping Journal*, Vol. 20 No. 1, pp. 69-76.

Sood A.K., Ohdar R.K. and Mahapatra S.S. (2009), "Parametric appraisal of fused deposition modelling process using the grey Taguchi method", *Proceedings IMechE Part B: Journal of Engineering Manufacture*, Vol. 224, pp. 135-145.

Taufik M., Jain P.K. (2016), "A study of build edge profile for prediction of surface roughness in fused deposition modeling", *ASME Journal of Manufacturing Science and Engineering*, Vol. 138, 061002.

Taufik M. and Jain P.K. (2017), "Characterization, modeling and simulation of fused deposition modeling fabricated part surfaces", *Surface Topography: Metrology and Properties*, Vol. 5, 045003.

Thrimurthulu K., Pandey P.M. and Reddy N.V. (2004), "Optimum part deposition orientation in fused deposition modeling", *International Journal of Machine Tools and Manufacture*, Vol. 44, pp. 585-594.

Tong K., Joshi S. and Lehtihet E.A. (2008), "Error compensation for fused deposition modeling (FDM) machine by correcting slice files", *Rapid Prototyping Journal*, Vol. 14 No. 1, pp. 4-14.

Turner B.N., Strong R. and Gold S.A. (2014), "A review of melt extrusion additive manufacturing processes: I. Process design and modeling", *Rapid Prototyping Journal*, Vol. 20 No. 3, pp. 192-204.

Turner B.N. and Gold S.A. (2015), "A review of melt extrusion additive manufacturing processes: II. Materials, dimensional accuracy and surface roughness", *Rapid Prototyping Journal*, Vol. 21 No. 3, pp. 250-261.

Vahabli E. and Rahmati S. (2017), "Hybrid estimation of surface roughness distribution in FDM parts using analytical modeling and empirical investigation", *International Journal of Advanced Manufacturing Technology*, Vol. 88, pp. 2287-2303.

Volpato N., Foggiatto J.A. and Schwarz D.C. (2014), "The influence of support base on FDM accuracy in Z", *Rapid Prototyping Journal*, Vol. 20 No. 3, pp. 182-191.

Wang C.C., Lin T.W. and Hu S.S. (2007), "Optimizing the rapid prototyping process by integrating the Taguchi method with the Gray relational analysis", *Rapid Prototyping Journal*, Vol. 13 No. 5, pp. 304-315.

Wang T.M., Xi J.T. and Jin Y. (2007), "A model research for prototype warp deformation in the FDM process", *International Journal of Advanced Manufacturing Technology*, Vol. 33, pp. 1087-1096.

Xinhua L., Shengpeng L., Zhou L., Xianhua Z., Xiaohu C. and Zhongbin W. (2015), "An investigation on distortion of PLA thin-plate part in the FDM process", *International Journal of Advanced Manufacturing Technology*, Vol. 79 No. 5, pp. 1117-1126.

Zhang Y. and Chou K. (2008), "A parametric study of part distortions in fused deposition modelling using three-dimensional finite element analysis", *Proceedings IMechE Part B: Journal of Engineering Manufacture*, Vol. 222, pp. 959-967.

Ziemian C.W. and Crawn P.M. III (2001), "Computer aided decision support for fused deposition modeling", *Rapid Prototyping Journal*, Vol. 7 No. 3, pp. 138-147.